

# The Andromeda Galaxy and Its Star Formation History

Denis Leahy 

Department of Physics and Astronomy, University of Calgary, Calgary, AB T2N 1N4, Canada; leahy@ucalgary.ca

**Abstract:** The state of knowledge of the properties of the Andromeda Galaxy (also known as M31) is reviewed. The spatial structure of the Andromeda Galaxy, its main source populations, and the properties of its gas and dust are discussed. To understand the formation history of the Andromeda Galaxy, the critical issues of its star formation history and the gas streams and dwarf galaxies in its surrounding environment are reviewed. Emphasis is on recent studies, with important earlier work described in the references provided here. It is important to understand the Andromeda Galaxy because it is the nearest large external galaxy and is close enough for high-resolution studies. This allows the Andromeda Galaxy to be used as a template for understanding more distant and less resolved galaxies in the universe.

**Keywords:** spiral galaxies; star formation; galactic structure; galaxy formation

## 1. Introduction

Star formation histories of galaxies are critically important for understanding the process of galaxy formation and the structure and contents of galaxies. Star formation can and has been studied in local galaxies for which the stellar populations are resolved and in more distant galaxies for which stars are unresolved, which are instead modeled as populations. Structural components of a galaxy can be resolved at much larger distances. The structural components include those long recognized, such as bulge, disk and halo. More recently recognized structures include separation of disks into thin and thick disk components and stellar streams, as well as recognition of significant numbers of dwarf companion galaxies. Stellar streams are the most recently recognized components of galaxies, mainly using observations of the Milky Way and the Andromeda Galaxy (M31).

In this overview, the properties of the Andromeda Galaxy/M31 are reviewed, including its star formation history, which informs us on the galaxy's formation and assembly. A recent study [1] focussed on the star formation of 36 nearby (distance < 4 Mpc) dwarf galaxies and concluded that local volume dwarf galaxies show evidence for synchronized formation of stars over the past 3 Gyr. Another study [2] considered the dust emission (100- to 500-micron wavelengths) of local group galaxies. Dust emission is used as a tracer of star formation because young stars are the primary heating source of the dust.

We focus on M31 because it is the nearest large spiral galaxy to the Milky Way, and it has several advantages over Milky Way studies. These include the unobscured view of M31, enabled because of M31's Galactic latitude (we do not need to look through the dust of the Milky Way disk), the well-known distances to stars and other objects in M31, and the global view of M31, which is not confused as is our inside view of the Milky Way.

M31 is also of interest because it is the most massive member of the local group, with the Milky Way as the only other massive galaxy. Using Gaia data [3], the motion of M31 relative to the Milky Way was determined using a significantly improved method than previously, confirming that the two massive galaxies are infalling toward their first close encounter.

Other related properties of M31, in addition to various measures of star formation history, are mentioned here. These are the structure of the galaxy, including bulge, disk, halo, and stellar streams, source populations in M31, its dust and gas content, and its



**Citation:** Leahy, D. The Andromeda Galaxy and Its Star Formation History. *Universe* **2023**, *9*, 349. <https://doi.org/10.3390/universe9080349>

Academic Editors: Marc S. Seigar, Giacomo Tommei, Gerald B. Cleaver, Marcello Abbrescia and Gonzalo J. Olmo

Received: 11 May 2023  
Revised: 1 July 2023  
Accepted: 24 July 2023  
Published: 26 July 2023



**Copyright:** © 2023 by the author. Licensee MDPI, Basel, Switzerland. This article is an open access article distributed under the terms and conditions of the Creative Commons Attribution (CC BY) license (<https://creativecommons.org/licenses/by/4.0/>).

surrounding environment (stellar streams and companion dwarf galaxies). Because high resolution- wide field ultraviolet (UV) observations have become available with GALEX [4] and the UVIT instrument [5] on AstroSat [6], UV measures of M31's star formation and galaxy structure are emphasized.

M31 is a giant spiral galaxy similar to the Milky Way but with roughly twice the mass. The galaxy's spiral structure is clearly seen in optical images (e.g., Figure 1), as are prominent dust lanes, especially NW of the central bulge. That the dust lanes are visible in the NW but not in the SE is a clear indicator that the NW disk is in front of the bulge and the SE disk is behind the bulge. This implies that the M31 rotation axis is tilted away from the observer in the NW and toward the observer in the SE. In Figure 1, two neighboring dwarf galaxies are also seen: NGC205 is NE of the bulge, just right of field F5, and M32 is in field F6, just west of center of that field.

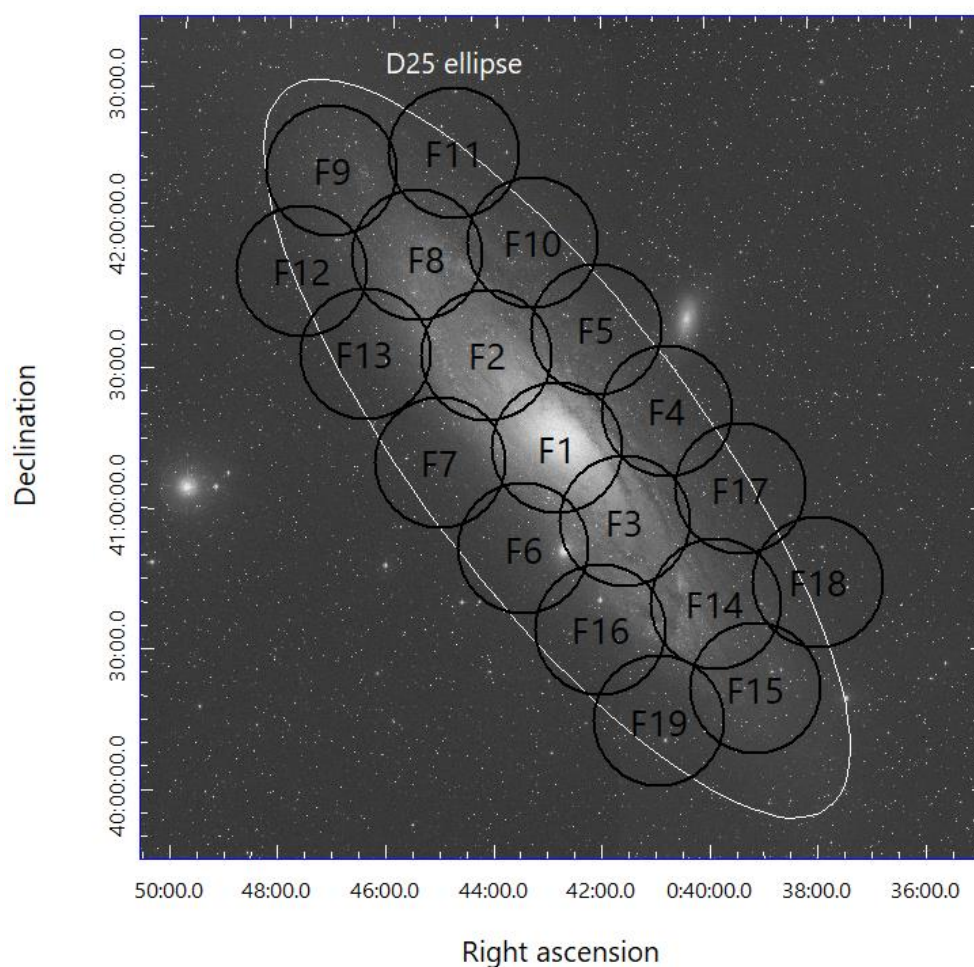


**Figure 1.** The greyscale image is the DSS J2000 blue filter image of M31. Right ascension and declination are J2000 coordinates. The white ellipse shows the D25 ellipse for M31, from [4]. The locations of the fields, F1 to F19, for the UVIT survey of M31 are shown by the black circles (from [7]). Note the prominent dust lanes that are in front of the bulge on the NW side of the center of M31.

For this review of M31, the areas of study are divided into five general topics. Section 2 discusses the structure of M31, and Section 3 lists the source populations in M31. Section 4 discusses the gas and dust in M31, and Section 5 describes what we know about the star formation history of M31. Section 6 discusses the environment of M31. By necessity, this review is not complete but focusses on work since about 2015, with the earlier work discussed in the provided references.

## 2. Structure of M31

M31 is an SAB-type spiral galaxy (see <https://ned.ipac.caltech.edu> accessed on 17 May 2023) with luminosity in the V band (visible) of  $3 \times 10^{10}$  solar (bolometric) luminosities. It has near-infrared luminosity of 1/3 of the V-band luminosity and far-infrared and ultraviolet luminosities about 1/30 and 1/60 of the V-band luminosity. The visible band image is shown in Figure 1 and is dominated by light from older stars, with some prominent dark lanes caused by absorption by dust in the interstellar medium. The ultraviolet and far-infrared images are shown in Figure 2 (left and right panels, respectively). Both images are dominated by the spiral arms, but for different reasons: the hot young stars in the spiral arms dominate the ultraviolet emission, whereas the far infrared is from the interstellar dust around the hot stars (and heated by those hot stars). The far-infrared luminosity is larger than the ultraviolet luminosity because most of the hot stars have significant extinction ( $A_{UV} \sim 0.5\text{--}5$  mag) from surrounding dust, which converts much of their ultraviolet luminosity into far-infrared radiation.

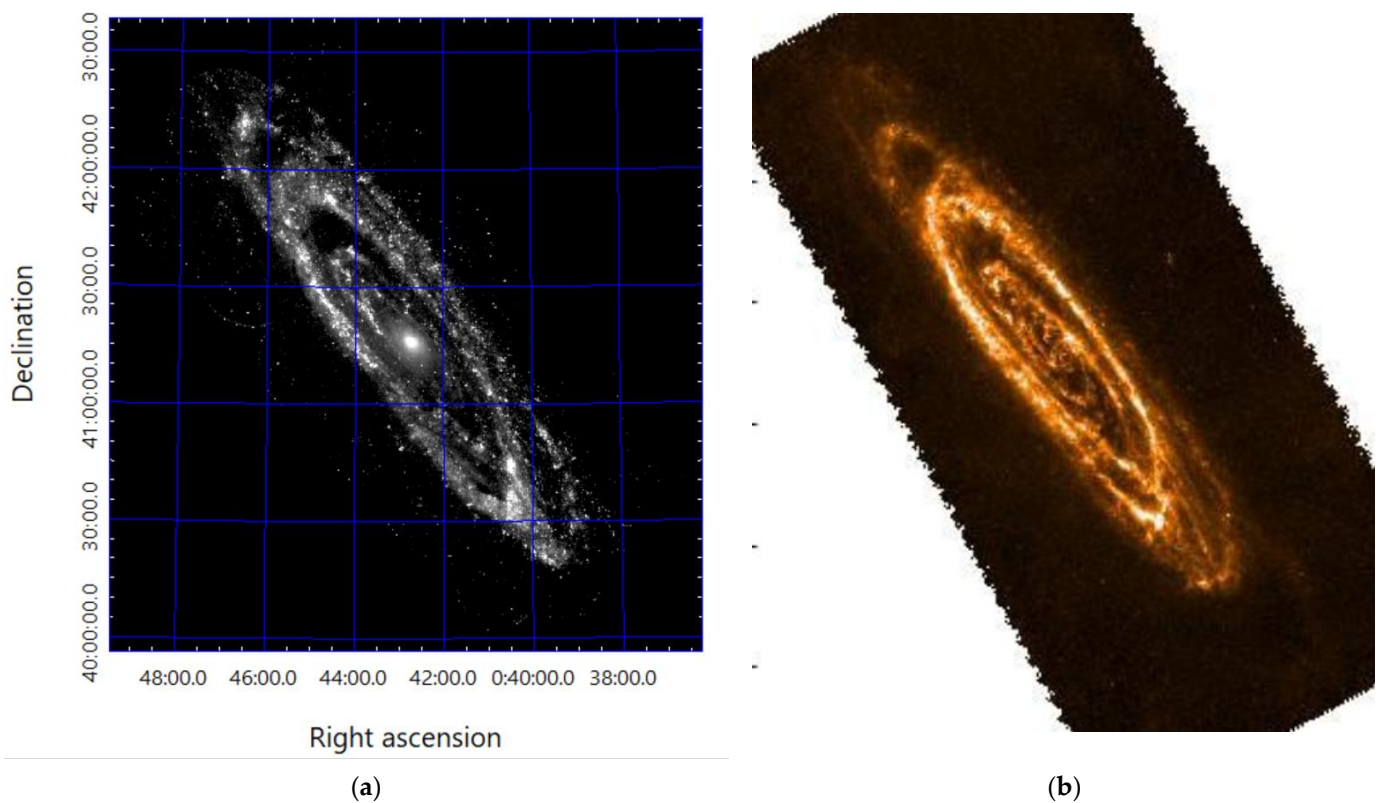


**Figure 2.** Images of M31 at ultraviolet and infrared wavelengths. (a) The 148 nm image of M31 [8]. (b) The far-infrared 250-micron image of M31 from the Hershel SPIRE instrument [9]. The ultraviolet and far-infrared images closely trace the spiral arms of M31. The ultraviolet and far-infrared emissions both closely follow the spiral arms and young stars of M31.

The major structures for spiral galaxies are present in M31: the disk, the central bulge, and the halo. The luminosity profile of M31 in near infrared (sensitive to stars and insensitive to dust) was modeled by [10] with the above three components. The main parameters were a disk scale length of 5.3 kpc, a bulge Sersic-function index of 2.2 and effective radius of 1 kpc, and a halo with a power-law profile with index  $-2.5$ . The kinematics of the disk stars and gas were analyzed by [11], showing that the offset in stellar and gas velocity increases with stellar age. They found that the use of a simple tilted ring model to explain the warps in the disk is inadequate.

The bulge is known to be triaxial and has been analyzed using N-body simulations [12]. To match the bulge properties, an initial classical bulge (ICB, which is formed by violent

relaxation early in the formation of the galaxy) with 1/3 of the total bulge mass and a Box/Peanut (B/P) bulge with 2/3 of the total bulge mass are required. The ICB (formed rapidly) and the B/P bulge (formed over Gyr) interact and evolve together [12]. The structure of the bulge in ultraviolet wavelengths was analyzed by [13]. The bulge was found to be complex with a boxy shape and found to require an eight-component model: three Sersic-function models for the main bulge and five components for the inner bulge and nuclear region. The asymmetry of M31's bulge and nuclear region requires this large number of components to model. Likely there are non-equilibrium components in the bulge related to the ongoing accretion of dwarf galaxies and stellar streams.

At the very center of M31 (radius < 4pc), there is a nuclear stellar disk orbiting the supermassive black hole [14]. The disk is tilted with respect to the large-scale galactic disk and exhibits a slow precession. This suggests that the nuclear cluster was formed from mass lost from old stars with eccentric orbits into the nuclear central region [15].

### 3. Source Populations in M31

M31 contains several types of sources, including point-like ones (stars and X-ray sources) and extended ones (globular clusters, open clusters, planetary nebulae, and supernova remnants). A number of star catalogs for M31 have been assembled (e.g., see references in [16]). The largest is from the Panchromatic Hubble Andromeda Treasury (PHAT), presented by [16], with 117 million stars. An ultraviolet catalog of sources in M31 was presented by [7], with ~80,000 sources, and many other catalogs for M31 can be found at the VizieR catalog library (<https://vizier.cds.unistra.fr/>). Far-ultraviolet variable stars were found by [17] using multi-epoch observations and identified with hot young stars.

373 X-ray sources and optical counterparts for half of them were studied by [18]. Half of the counterparts are background galaxies, the other half falling into several categories, including foreground stars, star clusters, and supernova remnants. The main problem with identifying optical counterparts is the intrinsic faintness of the X-ray sources at optical wavelengths. Ref. [19] identified 15 high-mass X-ray binaries and found that they are located in regions with young stars (less than 50 Myr old). Ultraviolet counterparts for 67 X-ray sources in M31 were found by [20], with the largest population being globular clusters. For the globular clusters, the ultraviolet emission was from blue horizontal branch stars in the cluster, whereas the X-ray emission was from an unrelated X-ray binary in the cluster.

The globular clusters are the oldest stellar populations and for the Andromeda Galaxy were found to consist of three major groups [21]: (1) an inner metal-rich group ( $[Fe/H] > -0.4$ ); (2) a group with intermediate metallicity (with median  $[Fe/H] = -1$ ); and (3) a metal-poor group, with  $[Fe/H] < -1.5$ . Here  $[Fe/H]$  is the log of the metal abundance (in this case, iron) relative to that of the Sun. The metal-rich globular cluster group has kinematics and spatial properties like those of the disk of M31, while the two more metal-poor cluster groups show mild prograde rotation overall.

Supernova remnants in M31 have been studied in a number of works ([8,22] and references therein). The number of supernova remnants (180) is dominated by those discovered by their optical emission lines, with 26 detected in X-rays [22]. The positions of the supernova remnants are closely associated with the spiral arms of M31 [8]. This is not surprising, because of the short lifetime of supernova remnants (~50,000 yr) and that  $\frac{3}{4}$  of them are from massive star explosions, so they are expected to form in the spiral arms. For the Milky Way, this association of spiral arms and supernova remnants is not possible to see because of the distance uncertainties of the remnants.

Planetary nebulae are useful for tracing the structure of the young thin disk and old thick disk of a galaxy, and their velocities can be used to trace the disk kinematics. For M31, [23,24] found that the thin disk and thick disk in M31 are two and three times as thick as the corresponding thin and thick disks in the Milky Way. The age-velocity dispersion relation derived from planetary nebulae in M31 indicates that a major merger of M31 with a satellite of 1/5 the mass of M31 took place 2.5 to 4.5 Gyr ago.

#### 4. Gas and Dust in M31

The gas and dust components of M31 are significant; as with many spiral galaxies, dark lanes in the disk are seen at optical wavelengths, which are caused by absorption by dust (Figure 1, northwest side of the disk). The neutral interstellar medium has been mapped in the 21 cm line of neutral hydrogen (HI). The recent work of [25] used high spatial and spectral resolution observations to study M31, finding observationally that HI spectra for most lines of sight are resolved into multi-component Gaussian line shapes. As a result, they found that corrections for optically thick HI have large uncertainties. This leads [25] to the conclusion that the opaque HI is better measured using absorption lines than emission lines.

Far-infrared maps were analyzed by [2] to determine dust mass, temperature, and luminosity maps for M31 and compare it to maps for M33 and the Large and Small Magellanic Clouds. Dust temperature and surface density were found to be higher for star-forming regions. By degrading the spatial resolution to mimic observations of more distant galaxies, they found that the temperature is systematically overestimated and the dust mass underestimated for the more distant galaxies. The effect is  $\sim 2$  K overestimate in dust temperature for clumpy galaxies like SMC, LMC, or M33 or  $\sim 1$  K for smooth galaxies like M31.

The dust distribution in the central bulge (radius  $< 700$  pc) of M31 was mapped by [26] using near-ultraviolet to near-infrared high-resolution imaging. The spectral energy distribution for each pixel was fit separately, allowing inference of the radial distance of each dust clump. The dust clumps were found to lie nearly in a plane that is roughly face-on. For supernova remnants in M31 [27], the dust temperature and mass were derived from fitting the near- to far-infrared spectral energy distributions. The dust surface density in supernova remnants was found to be half that in the surrounding regions, implying dust destruction by the supernova explosion.

Radiative transfer simulations to study the dust extinction in M31 were carried out by [28]. They reproduced the morphology and flux density from ultraviolet to sub-millimeter wavelengths, obtaining an attenuation curve consistent with previous estimates, and they found that 90% of the heating of the dust is caused by evolved stellar populations.

#### 5. Star Formation History of M31

The star formation history of M31 has been studied extensively, in large part because of the spatial resolution attainable; a typical resolution of 1 arcsecond is 3.8 pc at the distance of M31, and Hubble Space Telescope (HST) observations have 10 times finer resolution. Ref. [29] carried out a color-magnitude diagram (CMD) analysis of HST-resolved stars. This included both open clusters and field stars in part of the northeast disk of M31, with an upper age limit of  $\sim 300$  Myr on their sample. The cluster formation efficiency was found to vary across the disk, consistent with variations in mid-plane pressure. Models for cluster formation efficiency better reproduced observations when the gas depletion timescale was different for neutral hydrogen- and molecular hydrogen-dominated environments.

Ref. [30] developed the method of pixel CMD analysis to take into account partially resolved stellar populations and to be able to study the crowded bulk and disk regions of M31. Using seven age bins from  $10^6$  to  $10^{10}$  yr, they found a smooth exponential decay in star formation rate for the disk with a timescale of 4 Gyr and for the bulge with a 2 Gyr timescale. Ref. [31] derived ages, masses, and extinctions for 1363 star clusters in M31 observed with HST. They found that the mass function of clusters is compatible with mass functions found in other spiral galaxies, and it follows a Schechter function with a characteristic mass of  $10^5$  Solar masses. Ref. [32] measured the star formation history using HST observations of the northeast disk of M31. They fit CMDs to a large number of small regions (0.3 kpc by 1.4 kpc) and found that most stars formed prior to 8 Gyr ago, followed by a relatively quiet period until 4 Gyr ago, then with another star formation episode 2 Gyr ago, followed by recent quiescence.

The star formation history of the bulge of M31 was studied by [33] using HST CMDs. They found that more than 70 percent of the stars in the bulge are old (>5 Gyr) and metal-rich ([Fe/H]~0.3). At about 1 Gyr ago, there was a significant rise in star formation over the entire bulge region. For the central 130 arcsec (400 pc), there was an additional star formation episode less than 500 Myr old. Ref. [34] derived stellar population properties using Lick/IDS absorption line indices. The classical central bulge (<100 arcsec) was found to be old (11–13 Gyr) and metal-rich ([Fe/H]~0.3). The bar (extending out to 600 arcsec) is distinct in metallicity with near solar metallicity. The boxy-peanut component of the bulge also has near solar metallicity. The mass-to-light ratio of the above three components is the same, at 4.5 solar mass per solar luminosity. The disk of M31 (800 to 1600 arcsec from center) includes a mixture of ages, with the youngest at ~3–4 Gyr and with a mass-to-light ratio of 3 solar mass per solar luminosity.

Star formation studies of the bulge and disk were carried out using far-ultraviolet observations from the UVIT instrument with the method of spectral energy distribution fitting. Ultraviolet observations are particularly sensitive to the youngest (hottest) stars. Ref. [35] used total-light photometry to verify the result from [33] that the innermost bulge (100 arcsec) has a young stellar component of age ~100 Myr and a more recent star formation peak. The bulge was found to have a dominant old (10–12 Gyr) metal-rich ([Z/H]~0.3) population and a younger (600 Myr) solar abundance ([Z/H]~0) population throughout. For the innermost 120 arcsec, a very young (25 Myr) metal-poor ([Z/H]~-0.7) population was found. For the disk of M31 [36], 239 clusters in the northeast disk and bulge were modeled to measure ages, masses, metallicities, and extinctions. Cluster measurements are generally more sensitive to young populations than total light because the total light is diluted by the older field stars. Figure 3 (left panel) shows the locations of the clusters, with their ages indicated by the symbol size and color. Figure 3 (right panel) shows the ages of the clusters vs. their deprojected distance from the center of M31. The bulge has the oldest clusters, and the disk contains a mixture of two main age groups: one about 200 Myr old and a second about 4 Myr old. Both sets of clusters are associated with the spiral arms, and Figure 3a shows the younger clusters are more closely associated with the brightest parts of the arms.

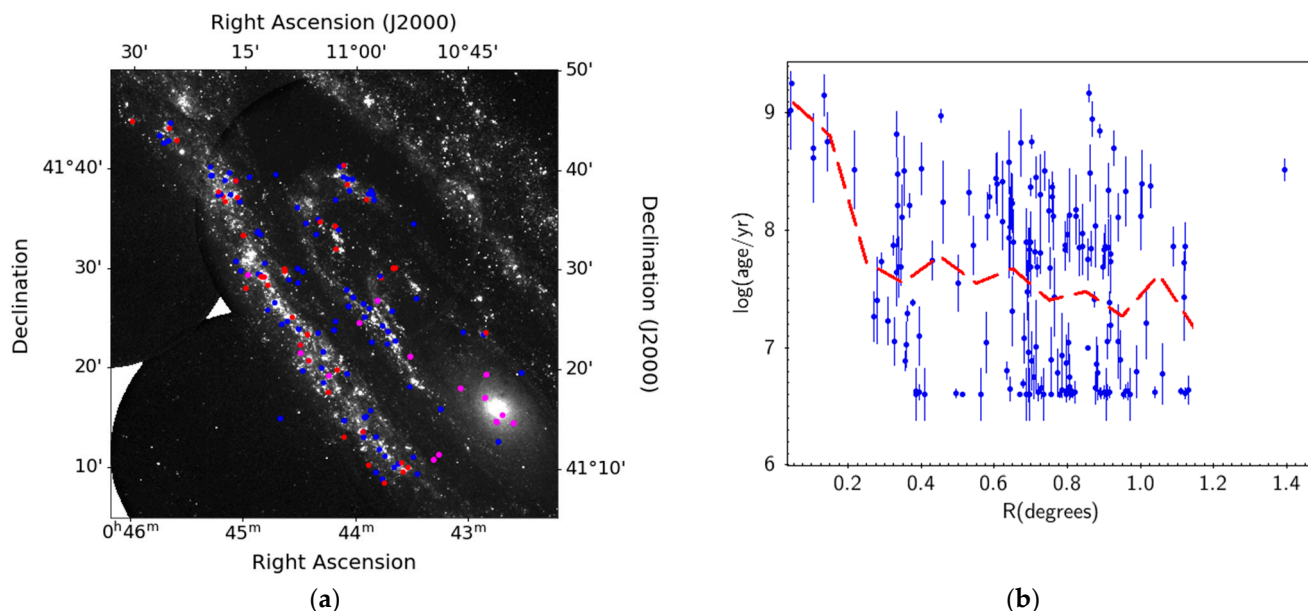


**Figure 3.** (a) Positions and ages of the clusters in the northeast disk and bulge of M31 studied by [36]. Log(age/yr) values are shown by the size of the circles, with radius proportional to log(age/yr) and total range 6.6 to 9.7. Clusters with log(age/yr) < 6.75 are plotted in red, 6.75 < log(age/yr) < 8.55 are shown in blue, and log(age) > 8.55 are shown in magenta. (b) Log(age/yr) of each cluster vs. deprojected distance from the center of M31 (blue symbols with error bars). The red dashed line shows the mean value for each bin. There are two distinct sets of cluster ages seen for R > 0.3°.

## 6. Surrounding Environment of M31

The standard picture of galaxy formation in an expanding universe includes a number of aspects, including the growth of density fluctuations in the presence of dark matter haloes. The scale and strength of the density fluctuations are derived from measurements of cosmic microwave background inhomogeneities. The density fluctuations result in the formation of the first mass concentrations and the first stars. The continued growth of the amplitude of density fluctuations results in the formation of the filamentary cosmic web, followed by the formation of large mass concentrations and galaxies at the intersection of filaments. Galaxies continue to grow as matter flows along the filaments onto the mass concentrations.

Various processes related to the growth and assembly of M31 have been studied by observing the surrounding environment of the galaxy. Here, recent work is summarized. Ref. [37] fits red giant branch stars in color-magnitude space to study M31's giant stellar stream and streams C and D. These streams are extended structures that are adjacent to M31 and are located on its southeast side. They are illustrated in Figure 3 of [37]. The metallicity of the stars for the giant stellar stream increases from  $-0.7$  to  $-0.2$  outward with distance from M31. Ref. [38] used data from the Pan-Andromeda Archaeological Survey, which covers more than  $400 \text{ degree}^2$ . They found that the 13 most distinctive substructures were produced by at least five different accretion events, all in the last 3 or 4 Gyr. The OPTICS clustering algorithm was used to quantify the hierarchical structure of M31's stellar halo and identify three new faint structures. The newer work by [39], using spectroscopy, did not confirm a metallicity gradient measured by  $[\alpha/\text{Fe}]$  in the giant stellar stream but found a high  $[\alpha/\text{Fe}]$  in the outer disk of M31, which is characteristic of rapid star formation induced by a major merger.

Simulations of M31 were carried out by [40] to explain recent observations that imply the disk was shaped by significant events 2–4 Gyr ago. The simulations lead to the conclusion that most of the halo substructure and complexity in the inner part of M31 can be caused by a single major interaction, for which the interacting galaxy has now merged with M31.

The circumgalactic medium (CGM) of M31 was studied by [41] using absorption line spectroscopy for 43 sightlines to background QSOs with impact parameters ranging from 25 to 570 kpc. The covering factor of Si III and O VI absorption lines was found to be near unity, showing that M31 has an extended ionized CGM ( $T \sim 10^4$ – $10^{5.5}$  K). The Milky Way likely has a similarly extended CGM, which extends far enough to overlap that of M31.

This review ends with a discussion of the satellite system of M31. The mass, metallicity, and velocity dispersion for 256 stars in five dwarf spheroidal satellites were derived from Keck spectroscopy by [42]. They showed that M31 and Milky Way satellites obey the same relation between mass and metallicity. The M31 dwarf spheroidal galaxies are more metal-poor than the giant stellar stream or the smooth inner halo [39,43]. This is consistent with the inner halo being the surviving remnants of more massive satellites that merged with M31 early in its history.

The missing satellites problem was studied using cosmological hydrodynamic models by [44]. At a fixed host mass of  $10^{12}$  solar masses, the simulations found a wide range of numbers of satellites. The number of satellites accreted was larger than the number of surviving satellites by a factor of 4–5; thus, they found that there is no missing satellites problem. The satellites in the local group are known to be located to within  $\sim 30$  degrees of a plane. Ref. [45] carried out cosmological simulations for Milky Way mass and M31 mass hosts to estimate the frequency of satellite positions that are near to a plane. They concluded that the coincidence of satellites lying near a plane is high enough that there is no plane-of-satellites problem.

## 7. Summary

In this review, the state of knowledge of the Andromeda Galaxy (M31) has been discussed, including its structure, source populations, gas and dust contents, star formation

history, and surrounding environment. An understanding of M31 is important because it is the nearest large galaxy to us, outside the Milky Way, and is amenable to detailed studies, which allow it to be used as a template for understanding more distant and difficult-to-observe galaxies in the universe.

**Funding:** This research was funded by the Canadian Space Agency, grant number 10036281.

**Data Availability Statement:** No new data were created or analyzed in this review article. Data sharing is not applicable to this article.

**Conflicts of Interest:** The author declares no conflict of interest. The funders had no role in the design of the study; in the collection, analyses, or interpretation of data; in the writing of the manuscript; or in the decision to publish the results.

## References

- Olsen, C.; Gawiser, E.; Iyer, K.; McQuinn, K.B.W.; Johnson, B.D.; Telford, G.; Wright, A.C.; Broussard, A.; Kurczynski, P. Star Formation Histories from Spectral Energy Distributions and Color-magnitude Diagrams Agree: Evidence for Synchronized Star Formation in Local Volume Dwarf Galaxies over the Past 3 Gyr. *Astrophys. J.* **2021**, *913*, 45. [[CrossRef](#)]
- Utomo, D.; Chiang, I.; Leroy, A.; Sandstrom, K.M.; Chastenet, J. The Resolved Distributions of Dust Mass and Temperature in Local Group Galaxies. *Astrophys. J.* **2019**, *874*, 141. [[CrossRef](#)]
- van der Marel, R.; Fardal, M.; Sohn, S.; Patel, E.; Besla, G.; del Pino, A.; Sahlmann, J.; Watkins, L.L. First Gaia Dynamics of the Andromeda System: DR2 Proper Motions, Orbits, and Rotation of M31 and M33. *Astrophys. J.* **2019**, *872*, 24. [[CrossRef](#)]
- Tandon, S.; Subramanian, A.; Girish, V.; Postma, J.; Sankarasubramanian, K.; Sriram, S.; Stalin, C.S.; Mondal, C.; Sahu, S.; Joseph, P.; et al. In-orbit Calibrations of the Ultraviolet Imaging Telescope. *Astrophys. J.* **2017**, *154*, 128. [[CrossRef](#)]
- Singh, K.; Tandon, S.; Agrawal, P.; Antia, H.M.; Manchanda, R.K.; Yadav, J.S.; Seetha, S.; Ramadevi, M.C.; Rao, A.R.; Bhattacharya, D.; et al. ASTROSAT mission. *Proc. SPIE* **2014**, *9144*, 91441S. [[CrossRef](#)]
- Gil de Paz, A.; Boissier, S.; Madore, B.; Seibert, M.; Joe, Y.H.; Boselli, A.; Wyder, T.K.; Thilker, D.; Bianchi, L.; Rey, S.; et al. The GALEX Ultraviolet Atlas of Nearby Galaxies. *Astrophys. J. Suppl. Ser.* **2007**, *173*, 185–255. [[CrossRef](#)]
- Leahy, D.; Postma, J.; Chen, Y.; Buick, M. AstroSat UVIT Survey of M31: Point-source Catalog. *Astrophys. J. Suppl. Ser.* **2020**, *247*, 47. [[CrossRef](#)]
- Leahy, D.; Monaghan, C.; Ranasinghe, S. Discovery of 20 UV-emitting SNRs in M31 with UVIT. *Astron. J.* **2023**, *165*, 116. [[CrossRef](#)]
- Herschel Data Search. Available online: <https://irsa.ipac.caltech.edu/applications/Herschel/> (accessed on 14 May 2023).
- Courteau, S.; Widrow, L.; McDonald, M.; Guhathakurta, P.; Gilbert, K.M.; Zhu, Y.; Beaton, R.L.; Majewski, S.R. The Luminosity Profile and Structural Parameters of the Andromeda Galaxy. *Astrophys. J.* **2011**, *739*, 20. [[CrossRef](#)]
- Quirk, A.; Guhathakurta, P.; Chemin, L.; Dorman, C.E.; Gilbert, K.M.; Seth, A.C.; Williams, B.F.; Dalcanton, J.J. Asymmetric Drift in the Andromeda Galaxy (M31) as a Function of Stellar Age. *Astrophys. J.* **2019**, *871*, 11. [[CrossRef](#)]
- Blana Diaz, M.; Wegg, C.; Ortwin, G.; Erwin, P.; Portail, M.; Opitsch, M.; Saglia, R.; Bender, R. Andromeda chained to the box—Dynamical models for M31: Bulge and bar. *Mon. Not. R. Astron. Soc.* **2017**, *466*, 4279–4298. [[CrossRef](#)]
- Leahy, D.; Craiciu, T.; Postma, J. The Complex Structure of the Bulge of M31. *Astrophys. J. Suppl. Ser.* **2023**, *265*, 6. [[CrossRef](#)]
- Lockhart, K.; Lu, J.; Peiris, H.; Rich, R.M.; Bouchez, A.; Ghez, A.M. A Slowly Precessing Disk in the Nucleus of M31 as the Feeding Mechanism for a Central Starburst. *Astrophys. J.* **2018**, *854*, 121. [[CrossRef](#)]
- Chang, P.; Murray-Clay, R.; Chiang, E.; Quataert, E. The Origin of the Young Stars in the Nucleus of M31. *Astrophys. J.* **2007**, *668*, 236. [[CrossRef](#)]
- Williams, B.; Lang, D.; Dalcanton, J. The Panchromatic Hubble Andromeda Treasury. X. Ultraviolet to Infrared Photometry of 117 Million Equidistant Stars. *Astrophys. J. Suppl. Ser.* **2014**, *215*, 9. [[CrossRef](#)]
- Leahy, D.; Buick, M.; Postma, J. Far-ultraviolet Variables in M31: Concentration in Spiral Arms and Association with Young Stars. *Astron. J.* **2021**, *162*, 199. [[CrossRef](#)]
- Williams, B.; Lazzarini, M.; Plucinsky, P. Comparing Chandra and Hubble in the Northern Disk of M31. *Astrophys. J. Suppl. Ser.* **2018**, *239*, 13. [[CrossRef](#)]
- Lazzarini, M.; Hornschemeier, A.; Williams, B. Young Accreting Compact Objects in M31: The Combined Power of NuSTAR, Chandra, and Hubble. *Astrophys. J.* **2018**, *862*, 28. [[CrossRef](#)]
- Leahy, D.; Chen, Y. AstroSat UVIT Detections of Chandra X-ray Sources in M31. *Astrophys. J. Suppl. Ser.* **2020**, *250*, 23. [[CrossRef](#)]
- Caldwell, N.; Romanowsky, A. Star Clusters in M31. VII. Global Kinematics and Metallicity Subpopulations of the Globular Clusters. *Astrophys. J.* **2016**, *824*, 42. [[CrossRef](#)]
- Sasaki, M.; Pietsch, W.; Haberl, F.; Hatzidimitriou, D.; Stiele, H.; Williams, B.; Kong, A.; Kolb, U. Supernova remnants and candidates detected in the XMM-Newton M 31 large survey. *Astron. Astrophys.* **2012**, *544*, A144. [[CrossRef](#)]
- Bhattacharya, S.; Arnaboldi, M.; Hartke, J.; Gerhard, O.; Comte, V.; McConnachie, A.; Caldwell, N. The survey of planetary nebulae in Andromeda (M 31). I. Imaging the disc and halo with MegaCam at the CFHT. *Astron. Astrophys.* **2019**, *624*, A132. [[CrossRef](#)]

24. Bhattacharya, S.; Arnaboldi, M.; Caldwell, N.; Gerhard, O.; Blaña, M.; McConnachie, A.; Hartke, J.; Guhathakurta, P.; Pulsoni, C.; Freeman, K.C. The survey of planetary nebulae in Andromeda (M 31). II. Age-velocity dispersion relation in the disc from planetary nebulae. *Astron. Astrophys.* **2019**, *631*, A56. [[CrossRef](#)]
25. Koch, E.; Rosolowsky, E.; Leroy, A.; Chasteney, J.; DaChiang, I.; Dalcanton, J.; A Kepley, A.; Sandstrom, K.M.; Schrubba, A.; Stanimirović, S.; et al. A lack of constraints on the cold opaque H I mass: H I spectra in M31 and M33 prefer multicomponent models over a single cold opaque component. *Mon. Not. R. Astron. Soc.* **2021**, *504*, 1801–1824. [[CrossRef](#)]
26. Dong, H.; Li, Z.; Wang, Q.; Lauer, T.R.; Olsen, K.A.G.; Saha, A.; Dalcanton, J.J.; Groves, B.A. High-resolution mapping of dust via extinction in the M31 bulge. *Mon. Not. R. Astron. Soc.* **2016**, *459*, 2262–2273. [[CrossRef](#)]
27. Wang, Y.; Jiang, B.; Li, J.; Zhao, H.; Ren, Y. The Dust Mass of Supernova Remnants in M31. *Astron. J.* **2022**, *163*, 60. [[CrossRef](#)]
28. Viaene, S.; Baes, M.; Tamm, A.; Tempel, E.; Bendo, G.; Blommaert, J.A.D.L.; Boquien, M.; Boselli, A.; Camps, P.; Cooray, A.; et al. The Herschel Exploitation of Local Galaxy Andromeda (HELGA). VII. A SKIRT radiative transfer model and insights on dust heating. *Astron. Astrophys.* **2017**, *599*, A64. [[CrossRef](#)]
29. Johnson, L.; Seth, A.; Dalcanton, J. Panchromatic Hubble Andromeda Treasury. XVI. Star Cluster Formation Efficiency and the Clustered Fraction of Young Stars. *Astrophys. J.* **2016**, *827*, 33. [[CrossRef](#)]
30. Conroy, C.; van Dokkum, P. Pixel Color Magnitude Diagrams for Semi-resolved Stellar Populations: The Star Formation History of Regions within the Disk and Bulge of M31. *Astrophys. J.* **2016**, *827*, 9. [[CrossRef](#)]
31. de Meulenaer, P.; Stonkutė, R.; Vansevičius, V. Deriving physical parameters of unresolved star clusters. V. M 31 PHAT star clusters. *Astron. Astrophys.* **2017**, *602*, A112. [[CrossRef](#)]
32. Williams, B.; Dolphin, A.; Dalcanton, J.; Weisz, D.R.; Bell, E.F.; Lewis, A.R.; Rosenfield, P.; Choi, Y.; Skillman, E.; Monachesi, A. PHAT. XIX. The Ancient Star Formation History of the M31 Disk. *Astrophys. J.* **2017**, *846*, 145. [[CrossRef](#)]
33. Dong, H.; Olsen, K.; Lauer, T.; Saha, A.; Li, Z.; García-Benito, R.; Schödel, R. The star formation history in the M31 bulge. *Mon. Not. R. Astron. Soc.* **2018**, *478*, 5379–5403. [[CrossRef](#)]
34. Saglia, R.; Opitsch, M.; Fabricius, M.; Bender, R.; Blaña, M.; Gerhard, O. Stellar populations of the central region of M 31. *Astron. Astrophys.* **2018**, *618*, A156. [[CrossRef](#)]
35. Leahy, D.; Seminoff, N.; Leahy, C. Far-ultraviolet to FIR Spectral-energy Distribution Modeling of the Stellar Formation History of the M31 Bulge. *Astron. J.* **2022**, *163*, 138. [[CrossRef](#)]
36. Leahy, D.; Buick, M.; Leahy, C. AstroSat/UVIT Cluster Photometry in the Northern Disk of M31. *Astron. J.* **2022**, *164*, 183. [[CrossRef](#)]
37. Conn, A.; McMonigal, B.; Bate, N.; Lewis, G.F.; Ibata, R.A.; Martin, N.F.; McConnachie, A.W.; Ferguson, A.M.N.; Irwin, M.J.; Elahi, P.J.; et al. Major substructure in the M31 outer halo: Distances and metallicities along the giant stellar stream. *Mon. Not. R. Astron. Soc.* **2016**, *458*, 3282–3298. [[CrossRef](#)]
38. McConnachie, A.; Ibata, R.; Martin, N.; Ferguson, A.M.N.; Collins, M.; Gwyn, S.; Irwin, M.; Lewis, G.F.; Mackey, A.D.; Davidge, T.; et al. The Large-scale Structure of the Halo of the Andromeda Galaxy. II. Hierarchical Structure in the Pan-Andromeda Archaeological Survey. *Astrophys. J.* **2018**, *868*, 55. [[CrossRef](#)]
39. Escala, I.; Gilbert, K.; Kirby, E.; Wojno, J.; Cunningham, E.C.; Guhathakurta, P. Elemental Abundances in M31: A Comparative Analysis of Alpha and Iron Element Abundances in the the Outer Disk, Giant Stellar Stream, and Inner Halo of M31. *Astrophys. J.* **2020**, *889*, 177. [[CrossRef](#)]
40. Hammer, F.; Yang, Y.; Wang, J.; Ibata, R.; Flores, H.; Puech, M. A 2–3 billion year old major merger paradigm for the Andromeda galaxy and its outskirts. *Mon. Not. R. Astron. Soc.* **2018**, *475*, 2754–2767. [[CrossRef](#)]
41. Lehner, N.; Berek, S.; Howk, J.; Wakker, B.P.; Tumlinson, J.; Jenkins, E.B.; Prochaska, J.X.; Augustin, R.; Ji, S.; Faucher-Giguère, C.-A.; et al. Project AMIGA: The Circumgalactic Medium of Andromeda. *Astrophys. J.* **2020**, *900*, 9. [[CrossRef](#)]
42. Kirby, E.; Gilbert, K.; Escala, I.; Wojno, J.; Kalirai, J.S.; Guhathakurta, P. Elemental Abundances in M31: The Kinematics and Chemical Evolution of Dwarf Spheroidal Satellite Galaxies. *Astron. J.* **2020**, *159*, 46. [[CrossRef](#)]
43. Gilbert, K.; Kirby, E.; Escala, I.; Wojno, J.; Kalirai, J.S.; Guhathakurta, P. Elemental Abundances in M31: First Alpha and Iron Abundance Measurements in M31’s Giant Stellar Stream. *Astrophys. J.* **2019**, *883*, 128. [[CrossRef](#)]
44. Engler, C.; Pillepich, A.; Pasquali, A.; Nelson, D.; Rodriguez-Gomez, V.; Chua, K.T.E.; Grebel, E.K.; Springel, V.; Marinacci, F.; Weinberger, R.; et al. The abundance of satellites around Milky Way- and M31-like galaxies with the TNG50 simulation: A matter of diversity. *Mon. Not. R. Astron. Soc.* **2021**, *507*, 4211–4240. [[CrossRef](#)]
45. Samuel, J.; Wetzel, A.; Chapman, S.; Tollerud, E.; Hopkins, P.F.; Boylan-Kolchin, M.; Bailin, J.; Faucher-Giguère, C.-A. Planes of satellites around Milky Way/M31-mass galaxies in the FIRE simulations and comparisons with the Local Group. *Mon. Not. R. Astron. Soc.* **2021**, *504*, 1379–1397. [[CrossRef](#)]

**Disclaimer/Publisher’s Note:** The statements, opinions and data contained in all publications are solely those of the individual author(s) and contributor(s) and not of MDPI and/or the editor(s). MDPI and/or the editor(s) disclaim responsibility for any injury to people or property resulting from any ideas, methods, instructions or products referred to in the content.